Fractional quantum Hall edge: Effect of nonlinear dispersion and edge roton

Shivakumar Jolad[1], Diptiman Sen[2], and Jainendra K. Jain[1]

[1] *Department of Physics, Pennsylvania State University, University Park, PA 16802 and*
[2] *Center for High Energy Physics, Indian Institute of Science, Bangalore 560012, India*

According to Wen's theory, a universal behavior of the fractional quantum Hall edge is expected at sufficiently low energies, where the dispersion of the elementary edge excitation is linear. A microscopic calculation shows that the actual dispersion is indeed linear at low energies, but deviates from linearity beyond certain energy, and also exhibits an "edge roton minimum." We determine the edge exponent from a microscopic approach, and find that the nonlinearity of the dispersion makes a surprisingly small correction to the edge exponent even at energies higher than the roton energy. We explain this insensitivity as arising from the fact that the energy at maximum spectral weight continues to show an almost linear behavior up to fairly high energies. We also formulate an effective field theory to describe the behavior of a reconstructed edge, taking into account multiple edge modes. Experimental consequences are discussed.

PACS numbers:

I. INTRODUCTION

The edge of a fractional quantum Hall (FQH) system [1] constitutes a realization of a chiral Tomonaga-Luttinger liquid (CTLL). (The word chiral implies that all the fermions move in the same direction). In a seminal work, Wen postulated that the CTLL at the FQH edge is very special in that the exponent characterizing its long-distance, low-energy physics is a universal quantized number, which depends only on the quantized Hall conductance of the bulk state but not on other details [2,3]. He described the FQH edge through an effective field theory approach (EFTA) based on the postulate that the electron operator at the edge of the $\nu = 1/m$ FQH state has the form

$$\hat{\psi}(x) \sim e^{-i\sqrt{m}\hat{\phi}(x)} \qquad (1)$$

where $\hat{\phi}(x)$ is the bosonic field operator. The imposition of antisymmetry forces m to be an odd integer [2], which, in turn, leads to quantized exponents for various correlation functions. In particular, it predicts a relation $I \sim V^3$ between the current (I) and the voltage (V) for tunneling from a three-dimensional Fermi liquid into the 1/3 FQH edge, which has been tested experimentally by Chang *et al.* and Grayson *et al.* [4–7].

Wen's theory describes the FQHE edge in the asymptotic limit of low energies and long distances. The CTLL description is inapplicable at energies comparable to or larger than the bulk gap, where bulk excitations become available; we will not consider such high energies in this work. However, even in a range of energies below the bulk gap, deviations from the ideal asymptotic behavior may arise because the dispersion of the elementary edge excitation deviates from linearity and also exhibits an "edge roton minimum." The aim of this paper is to estimate these corrections from a microscopic approach. To focus on these corrections, we make appropriate approximations (mainly a neglect of composite fermion Λ

level mixing, discussed previously [8]) that guarantee an ideal quantized behavior at very low energies.

A deviation from linearity in the dispersion of the elementary edge excitation is expected to produce corrections for the following reason. In the bosonic model of edge excitations, the spectral weights of all excitations at a given momentum obey a sum rule (see Eq. (20)), first demonstrated by Palacios and MacDonald [9], which is valid up to a unitary rotation of the basis. The long time behavior of the Green function and the differential conductance for tunneling from an external Fermi liquid into the FQH edge, on the other hand, are sensitive to the states within an energy slice. However, for linear dispersion, the energy and momentum are uniquely related, so the sum rule is also valid for all states at a given *energy*, which produces a quantized power law exponent for the differential conductance. (A more detailed discussion is given in Appendix B). A nonlinearity in the dispersion, on the other hand, produces an energy band for excitations, as shown, for example, in Fig. 6 below. In the absence of a unique relation between energy and momentum, the spectral weight sum rule is now valid for all states at a given momentum but not for all states at a given energy, and there is no reason to expect the same power law behavior as that at low energies.

In this paper, we compute the edge spectral function from a microscopic approach using the method of composite fermion (CF) diagonalization, wherein we consider a truncated basis of states that contain no pairs of electrons with angular momentum unity. These are the only states that survive when the Haldane pseudopotential [10,11] V_1 is taken to be infinitely strong; all states containing pairs with angular momenta equal to unity are pushed to infinity. Laughlin's 1/3 wave function [12] is exact for this model. Restriction to this subspace is also tantamount to considering edge excitations within the lowest Λ level (or CF Landau level). A neglect of Λ level mixing has been shown to be very accurate for the bulk physics, and we explicitly confirm below, by comparison

to exact diagonalization results for small systems, that it provides a good first approximation for the edge excitations as well. Restricting to this truncated basis allows us to study systems with a large number of particles, providing better thermodynamic estimates than were available previously.

We determine the thermodynamic limit of the dispersion of the elementary edge excitation. Our results show that while it is linear at low energies, it begins to deviate from linearity at an energy that is a fraction the 1/3 bulk gap. It also exhibits a roton minimum, which vanishes at a critical setback distance signaling edge reconstruction, in agreement with previous work [13,14]. We show that while the spectral weights of individual excitations depend on various parameters [14], they accurately obey the sum rule mentioned above over the entire parameter range that we have studied.

To determine the effect of the nonlinear dispersion on the edge exponent we employ a hybrid approach described in Sec. V, wherein we build the spectrum from the elementary edge boson with a nonlinear dispersion but assume the spectral weights of the EFTA model. We evaluate the tunneling $I - V$ characteristic and find that the calculated exponent remains unchanged to a very good approximation even at energies above the edge roton energy where the dispersion is nonlinear. Zülicke and MacDonald [15] have also calculated the spectral function and the $I - V$ characteristics for a $\nu = 1/3$ edge by assuming a dispersion $\epsilon(q) \sim -q \ln(\alpha q)$ for the edge magnetoplasmon, where q is the momentum and α is a constant; they have found that the edge exponent varies as the inverse filling. Our calculation is based on a magnetoplasmon dispersion that is obtained from a microscopic calculation for a system with Coulomb interaction and a realistic confinement potential. Recently, the effect of a nonlinearity of the fermionic spectrum on the long-distance, low-energy correlation functions has been studied in Refs. [16,17]. However, this analysis considers a system in which both right and left-moving modes are present and interact with each other, and it is not clear whether the same analysis would be applicable to a FQH edge with a single chiral mode.

One may also expect some signature in tunnel transport that may be associated with the edge roton, which would then allow such transport to serve as a spectroscopic probe of the edge roton. However we find that the effect of edge roton on tunnel transport is negligible, because the spectral weight in the edge roton mode is very small.

Our paper is organized as follows. Section II contains a description of the model and the method of calculation. In Sec. III, we evaluate the energy spectra for small systems and compare them with the exact results. In Sec. IV, we study large systems and extract the thermodynamic edge dispersion, edge reconstruction and the edge roton. In Sec. V, we calculate the spectral weights and the associated sum rules for the EFTA, and we test the validity of these rules for the electronic spectra. We also outline our hybrid approach to calculate spectral function and tunneling density of states. In Sec. VI, we calculate the spectral function and tunneling density of states, present our main results on the $I - V$ characteristics, and mention their implications for the robustness of the edge exponent under a nonlinear dispersion. In Sec. VII, we discuss a system with a reconstructed edge using a field theoretic approach and address the effect on the tunneling exponent. We conclude in Sec. VIII with a summary and a discussion of the causes and implications of our main results. In the Appendix we give a mathematical formalism for the spectral weights, sum rules, and the Green's functions for an ideal and a non-ideal EFTA.

II. MODEL AND METHOD OF CALCULATION

A. Hamiltonian

We consider a two-dimensional electron system in a plane. The confinement is produced by a neutralizing background with uniformly distributed positive charge in a disk (denoted Ω_N) of radius $R_N = (\sqrt{2N/\nu})\, l$; here N is the number of electrons, ν is the filling factor, and $l = \sqrt{\hbar c/eB}$ is the magnetic length. (The symbol l is also used for angular momentum later, but the meaning ought to be clear from the context.) The background charge disk is separated from the electron disk by a setback distance d. The ground state of the electron is determined by a microscopic calculation; we expect the electrons to be approximately confined to a disk of radius R_N to ensure charge neutrality in the interior. This system is modeled by the following Hamiltonian:

$$
\begin{aligned}
H \;\equiv\;& E_{\mathrm{K}} + V_{\mathrm{ee}} + V_{\mathrm{eb}} + V_{\mathrm{bb}} \\
=\;& \sum_j \frac{1}{2m_b}\left(\boldsymbol{p}_j + \frac{e}{c}\boldsymbol{A}_j\right)^2 + \sum_{j<k}\frac{e^2}{\epsilon|\boldsymbol{r}_j - \boldsymbol{r}_k|} \\
& -\rho_0 \sum_j \int_{\Omega_N} d^2 r \frac{e^2}{\epsilon\sqrt{|\boldsymbol{r}_j - \boldsymbol{r}|^2 + d^2}} \\
& +\rho_0^2 \int_{\Omega_N}\int_{\Omega_N} d^2 r\, d^2 r' \frac{e^2}{\epsilon|\boldsymbol{r}' - \boldsymbol{r}|},
\end{aligned}
\tag{2}
$$

where the terms on the right hand side represent the kinetic, electron-electron, electron-background, and background-background energies, respectively. Here m_b is the band mass of the electrons, $\boldsymbol{p}_j$ is the momentum operator of the jth electron and $\boldsymbol{r}_j$ is its position, $\boldsymbol{A}_j$ is the vector potential at $\boldsymbol{r}_j$, $\rho_0 = \nu/2\pi l^2$ is the positive charge density spread over a disk of radius R_N, and ϵ is the dielectric constant of the background semiconductor material. At large magnetic fields, only the lowest Landau level states are occupied; hence the kinetic energy $\hbar\omega_c/2$ (where $\omega_c \equiv eB/m_b c$ is the cyclotron frequency) is a constant which will not be considered explicitly.

B. Electron States

The single particle states in the nth Landau level are given, in the symmetric gauge, by

$$\eta_{n,m}(z) = \frac{(-1)^n}{\sqrt{2\pi}} \sqrt{\frac{n!}{2^m(m+n)!}} e^{-r^2/4} z^m L_n^m \left(\frac{r^2}{2} \right),$$
(3)

where $L_n^m(x)$ is the associated Laguerre polynomial [18], n and m denote the Landau level index and angular momentum index respectively, $z = x - iy$ represents the electron coordinates in the complex plane, $r = |z|$, and all lengths are quoted in units of the magnetic length l. The lowest Landau level states ($n = 0$) are of special importance for our calculations below; they are given by

$$\eta_{0,m}(z) = \frac{z^m e^{-|z|^2/4}}{\sqrt{2\pi 2^m m!}}.$$
(4)

The many-body states are formed by taking linear combinations of antisymmetric products of single particle wave functions denoted by $|p_1, p_2, \cdots p_N\rangle = a_{p_1}^\dagger a_{p_2}^\dagger \cdots a_{p_N}^\dagger |0\rangle$, where $p_i = \{n_i, m_i\}$ is the single particle state index of the ith electron, and $a_{p_i}^\dagger$ is the corresponding creation operator. We will be interested in the edge excitations of the FQH state at $\nu = 1/3$ below. The ground state has total angular momentum $M_0 = 3N(N-1)/2$. The angular momentum of the excited state, ΔM, will be measured relative to M_0.

C. Models of FQH Edge

The tunneling of electrons from a two-dimensional electron gas into a Fermi liquid (such as a metal or $n+$ doped GaAs) has been studied experimentally in two geometries: point-contact geometry and cleaved-edge-overgrowth geometry [7]. These are believed to represent realizations of smooth and sharp edges, respectively [19].

In the point-contact geometry, the boundary of the two-dimensional electron gas is smooth. Theoretically a smooth edge can be modeled by including all possible many-body edge excitation states for a given total angular momentum M ($= \sum_{i=1}^N m_i$), placing no restrictions on the maximum single particle angular momentum m_i. The smoothness is ensured by states extending a few magnetic lengths beyond the disk edge.

The cleaved-edge geometry is characterized by a long and thin tunneling barrier with a typical barrier width of about one magnetic length. Recent experiments suggest that the cleaved-edge-overgrowth represents the realization of a sharp quantum Hall edge [19]. A sharp edge can be modeled [13] by excluding the single particle angular momenta beyond a cutoff m_{max}, given by

$$m_{max} = 3(N - 1) + l_0,$$
(5)

where l_0 is taken to be a small integer.

We have calculated the edge spectra for both smooth edge and sharp edge, with cutoff $l_0 = 2$. We show in Sec. III, that the low-energy branch of the sharp edge matches with that of the smooth edge, and hence the edge dispersion is not very sensitive to this issue. The calculations for the spectral functions are carried out for a smooth edge only. We note that a sharp edge eliminates several higher energy states, but does not significantly affect the low-energy branch and hence edge reconstruction.

D. Exact Diagonalization

The exact interaction energy for FQH systems can be calculated for small systems using numerical diagonalization techniques. In the disk geometry with symmetric gauge, for a given total angular momentum M, the basis states $|m_1, m_2, \cdots m_N\rangle$ in the lowest Landau level are generated according to the conditions:

$$\sum_j m_j = M; \quad 0 \le m_1 < m_2 \cdots < m_N.$$
(6)

Restricting to the lowest Landau level, the Hamiltonian in the second quantized representation is

$$H = \frac{1}{2} \sum_{r,s,t,u} \langle r, s|V_{ee}|t, u\rangle a_r^\dagger a_s^\dagger a_t a_u$$
$$+ \sum_m \langle m|V_{eb}|m\rangle a_m^\dagger a_m + V_{bb}.$$
(7)

Here the electron-electron and electron-background interaction matrix elements are defined as

$$\langle r, s|V_{ee}|t, u\rangle = \int d^2r_1 d^2r_2 \eta_r^*(r_1)\eta_s^*(r_2)\frac{e^2}{\epsilon r_{12}}\eta_t(r_1)\eta_u(r_2);$$

$$\langle m|V_{eb}|m\rangle = -\rho_0 \int d^2r_1 \int_{\Omega_N} d^2r_2 \frac{|\eta_m(r_1)|^2}{\sqrt{r_{12}^2 + d^2}},$$
(8)

with $r + s = t + u$.

The background-background interaction energy per particle is calculated analytically to be

$$\frac{\langle V_{bb}\rangle}{N} = \frac{\rho_0^2}{2N} \int_{\Omega_N} d^2r \int_{\Omega_N} d^2r' \frac{e^2}{\epsilon|\boldsymbol{r} - \boldsymbol{r}'|} = \frac{8}{3\pi}\sqrt{\frac{\nu N}{2}},$$
(9)

with the energy measured in units of $e^2/\epsilon l$. This adds a constant term to the matrix elements of the Hamiltonian. (The constant background-background interaction must be included to obtain a sensible thermodynamic limit for the energy, but is irrelevant for energy *differences*). Computing the electron-background interaction $\langle V_{eb}\rangle$ requires numerical integration. To this end, we can
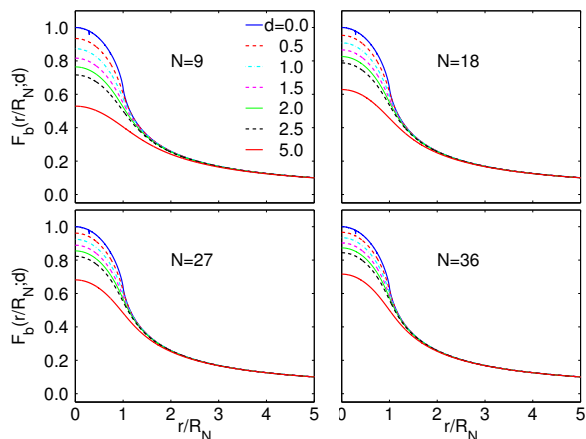
FIG. 1: (Color online) The function $F_b(r_i/R_N; d)$ that appears in the expression for the electron-background energy (Eq. (10)) for several values of d and N. Here r is the distance of the electron from the center of the disk, and R_N is the radius of the disk of the neutralizing positive background charge.

write the electron-background energy as

$$V_{\rm eb} = \sum_{i=1}^{N} v_{eb}(\boldsymbol{r}_i);$$

$$v_{eb}(\boldsymbol{r}_i) = -\rho_0 \int_{\Omega_N} d^2 r \frac{e^2}{\epsilon\sqrt{|\boldsymbol{r}_i - \boldsymbol{r}|^2 + d^2}}$$

$$\equiv -\sqrt{2\nu N} F_b(r_i/R_N; d). \qquad (10)$$

For $d = 0$, the integral in Eq. (10) on the right hand side can be calculated analytically, the result of which has been given by Ciftja and Wexler [20]. For $d \neq 0$, numerical integration is necessary. Figure 1 shows plots of the function F_b for different d and N.

For the electron-electron interaction, we find the analytical expressions for $\langle r, s | V_{\rm ee} | t, u \rangle$ given by Tsiper in Ref. [21] to be useful. It is then straightforward to construct the Hamiltonian matrix and diagonalize it either by using standard diagonalization procedures for small systems ($N \leq 7$) to get the full spectrum, or by the Lanczos algorithm for slightly larger systems ($N = 8, 9$) to get the low-energy spectrum. In the present work, we have performed full diagonalization for systems with up to 7 particles.

E.   CF diagonalization

We exploit the fact that the CF theory produces very accurate wave functions for low-energy eigenstates of the problem. Our approach will be to construct a truncated

basis for the wave functions for the edge excitations [11, 22], and then diagonalize the full Hamiltonian within this basis to obtain various quantities of interest. The method has been described in detail in the literature [8,23,24], so we present only a brief outline here.

For the fraction $\nu = n/(2np + 1)$, the CF theory maps interacting electrons at total angular momentum M to non-interacting composite fermions at $M^* = M - pN(N-1)$ [25,26] by attaching $2p$ flux quantum to each electron. The ansatz wave functions Ψ_α^M for interacting electrons with angular momentum M are expressed in terms of the known wave functions of non-interacting electrons $\Phi_\alpha^{M^*}$ at M^* as follows:

$$\Psi_\alpha^M = \mathcal{P}_{\rm LLL} \prod_{j<k} (z_j - z_k)^{2p} \Phi_\alpha^{M^*}. \qquad (11)$$

Here $\alpha = 1, 2, \cdots, D^*$ labels the different states, $\mathcal{P}_{\rm LLL}$ denotes projection into the lowest LL, and D^* is the dimension of the CF basis. We choose $p = 1$ as appropriate for $\nu = 1/3$, and restrict $\Phi_\alpha^{M^*}$ to states with the lowest kinetic energy at M^*. No lowest Landau level projection is required for these states, as they are already in the lowest Landau level.

The Landau levels at M^* transform into Landau-like effective kinetic energy levels of composite fermions, called Λ levels. The restriction to the lowest Landau level at M^* is equivalent to restricting composite fermions to their lowest Λ level. More accurate spectra can be obtained by allowing Λ level mixing and performing CF diagonalization (CFD) in a larger space, but that will not be pursued here. As will be seen below, the lowest Λ level results are sufficiently accurate for our purposes.

The advantage of CF diagonalization is that the dimension D^* of the CF basis is much smaller than the dimension of the full lowest Landau level Hilbert space at M; this allows a study of much larger systems. Table I compares the dimensions of the full Hilbert space (D) and the truncated CF space (D^*) for 6 to 12 particles for several values of ΔM. The dimension D increases exponentially, approximately as $D = 10^{-2}\exp(2N)$ for large N. This gives $D \approx 2 \times 10^{29}$ for $N = 36$ particles, in dramatic contrast to $D^* \sim$ 10-100 for $0 \leq \Delta M < 10$. Of course, the Hilbert space reduction comes with a cost: the CF basis functions are much more complicated than the usual single Slater determinant basis functions, and diagonalization of the Hamiltonian in this basis requires many non-trivial steps and extensive Monte Carlo. Nonetheless, CF diagonalization can be, and has been, performed for many non-trivial cases of interest.

We need to evaluate the matrix elements of the Hamiltonian in our CF basis. If $\Psi_\alpha^M(z_1, z_2, \cdots, z_N)$ and $\Psi_\beta^M(z_1, z_2, \cdots, z_N)$ denote two CF states at angular momentum M, then the electron-background and electron-electron energy matrix elements are given by $\langle \Psi_\alpha^M | V_{\rm eb} | \Psi_\beta^M \rangle$ and $\langle \Psi_\alpha^M | V_{\rm ee} | \Psi_\beta^M \rangle$. Their evaluation requires evaluating multi-dimensional integrals, which can be effectively accomplished by Monte Carlo techniques described in the next section. The CF basis functions

ΔM	$D(N=6)$	$D(N=7)$	$D(N=8)$	$D(N=9)$	$D(N=10)$	$D(N=11)$	$D(N=12)$	D^*
0	1,206	8,033	55,974	403,016	2,977,866	22,464,381	172,388,026	1
1	1,360	8,946	61,575	439,100	3,218,412	24,117,499	184,030,746	1
2	1,540	9,953	67,696	478,025	3,476,314	25,879,361	196,384,297	2
3	1,729	11,044	74,280	519,880	3,752,096	27,755,663	209,483,911	3
4	1,945	12,241	81,457	564,945	4,047,402	29,753,578	223,373,383	5
5	2,172	13,534	89,162	613,331	4,362,833	31,879,397	238,091,562	7
6	2,432	14,950	97,539	665,355	4,700,201	34,141,000	253,686,437	11
7	2,702	16,475	106,522	721,125	5,060,174	36,545,347	270,200,645	15
8	3,009	18,138	116,263	780,997	5,444,732	39,101,065	287,686,698	22

TABLE I: Dimension D of the full Hilbert space (used in exact diagonalization) for several values of N and ΔM. Here ΔM is the angular momentum measured relative to the angular momentum $M_0 = 3N(N-1)/2$ of the ground state of the $\nu = 1/3$ FQH state. The last column gives D^*, the dimension of the CF basis in the lowest Λ level, used in our CF diagonalization. The values of D^* are given for sufficiently large N where they are N independent; for small N, D^* may be smaller than the given value.

are in general not orthogonal to each other. They can be orthogonalized by the Gram-Schmidt procedure adapted for CF states to produce the energy spectrum as described in the literature [8,11,23,24]. Essentially, given the interaction matrix $\hat{V}_{\alpha,\beta} = \langle \Psi_\alpha | V | \Psi_\beta \rangle$ and the overlap matrix $\mathcal{O}_{\alpha,\beta} = \langle \Psi_\alpha | \Psi_\beta \rangle$, the energies and eigenvalues are obtained by diagonalizing the matrix $\mathcal{O}^{-1}\hat{V}$.

F. Monte Carlo Methods

Multi-dimensional integrals can be evaluated most effectively by the Metropolis-Hastings Monte Carlo (MHMC) algorithm [27–29]. For a discussion of the application of MHMC algorithm to quantum many-body systems, in particular to quantum Hall systems, we refer the reader to Refs. [11,20]. For our energy calculations, we find it sufficient to thermalize for 100,000 iterations and then average over about $10 - 20$ million iterations for each angular momentum. For spectral weights calculations, about 200 million iterations are required for the eigenvector. These numbers do not vary significantly with N in the range of our study ($N \leq 45$), but the computation time increases exponentially with N and ΔM, limiting our study to systems up to $N = 45$ particles for the energy spectrum, and $N = 27$ for spectral weights. The energies were calculated for $\Delta M = 1 - 8$ and the spectral weights for $\Delta M = 1 - 4$.

III. SMALL SYSTEM STUDIES

The CFD approach has been well tested in the past for the *bulk* physics at various filling factors and has been shown to capture the behavior of FQH systems accurately. Before proceeding to larger systems, we first test the validity of the CFD approach for the edge excitations.

Using the CF diagonalization procedure outlined earlier, we compute the edge excitation spectra for the $\nu = 1/3$ state for several parameters in the range $d = 0$-$2.5l$ and $\Delta M = 0$-8. Figures 2 and 3 show comparisons of
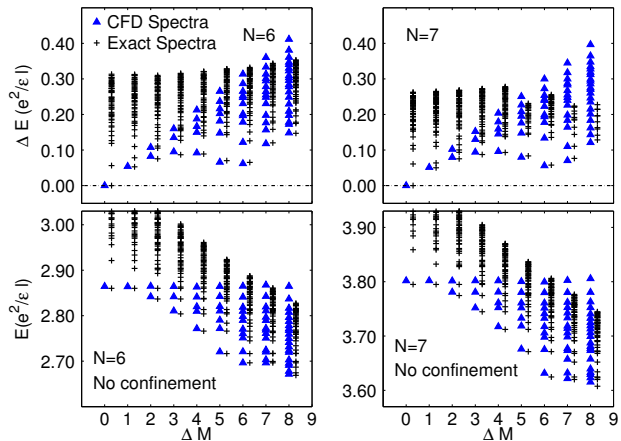

FIG. 2: (Color online) Comparison of CFD spectra with the exact spectra for the smooth edge for 6 and 7 particles, with and without a positive background (upper panels and lower panels, respectively). For the upper panels, we have taken $d = 0$. Blue triangles are the energies obtained by CF diagonalization, and the adjacent '+' symbols (shifted along the x axis for clarity) are the exact energies. The high energy parts of the exact spectrum are not shown. All energies are quoted in units of $e^2/\epsilon l$, and are measured relative to the energy of the ground state at $\Delta M = 0$. ΔM is the angular momentum of the excitation.

the CFD spectra with the exact spectra for smooth and sharp edges (exact diagonalization is possible for slightly larger systems for a sharp edge because of the additional restriction on the Fock space), demonstrating that the CFD approach is essentially exact. For a sharp edge, we have chosen the value $l_0 = 2$ (cf. Eq. (5)). The exact diagonalization results in Fig. 3 are taken from Wan *et. al* [13]. Consistent with their conclusions, we find that edge reconstruction occurs for d greater than a critical separation.

We note that for small systems the results for sharp and smooth edges are not very different, as shown in Fig. 4; both show edge reconstruction for $d > 1.5l$. For
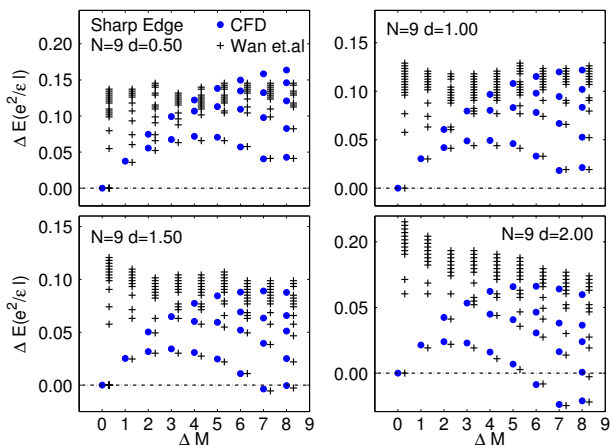
FIG. 3: (Color online) Comparison of the CFD spectra with the exact spectra for a sharp edge for $N = 9$ particles at $\nu = 1/3$ with $d = 0.5 - 2.0$ l. Blue dots indicate the energies obtained by CF diagonalization, whereas the adjacent '+' symbols (shifted along the x axis for clarity) are energies extracted from the figures of Ref. [13].

larger systems, as seen below, edge reconstruction occurs for larger d for the sharp edge as expected.

IV.   SPECTRA AND EDGE DISPERSION

Having ascertained the validity of our approach from comparisons to exact results, we now proceed to investigate the physics in the thermodynamic limit. We study the edge spectra for different sizes and approach the thermodynamic limit by identifying a scaling relation between the physical momentum δk (we take $\hbar = 1$) and the edge angular momentum ΔM. The momentum is related to the size of the system by $k \sim r/l^2$, where r is the radius of the orbital wave function. For edge electrons, $r = \sqrt{2Ml} = \sqrt{2(3(N-1) + \Delta M)}l$ for a system with $\nu = 1/3$. This gives the momentum of the edge excitation to be

$$\delta k = \frac{\Delta M}{\sqrt{6(N-1)}l}. \tag{12}$$

Henceforth we will denote δk, the physical momentum of the edge excitation, as simply k.

Based on our edge spectra results in Fig. 5, with the parameters $N = 6 - 36$, $d = 0$-$2.5l$, and $\Delta M = 0$-8, we make the following observations.

i. **Data Collapse**: The energy spectra for different system sizes collapse, indicating proper scaling to the thermodynamic limit. The lowest branch in each of the four panels corresponds to the dispersion of the single edge boson, for various setback distances in the range $d = 0 - 2.5l$. The data collapse to a single curve is apparent even for
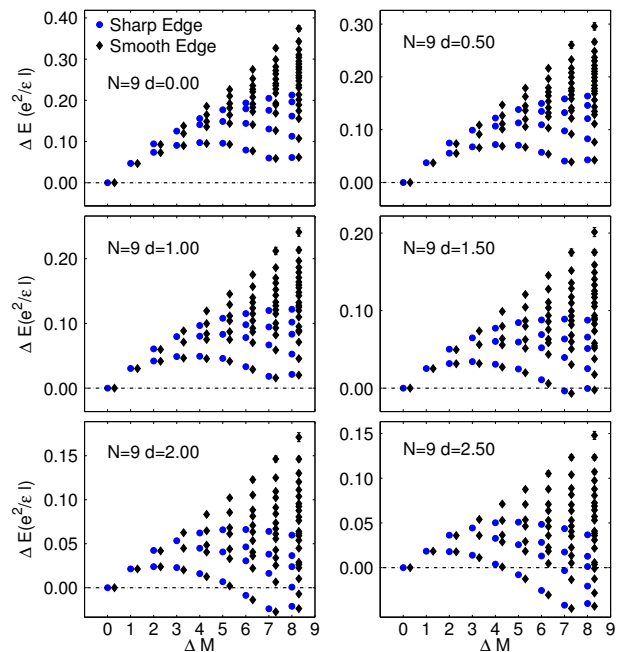

FIG. 4: (Color online) Energy spectra for smooth and sharp edge excitations of a $\nu = 1/3$ system with $N = 9$ and $d = 0.0 - 2.5$ l. Blue dots are for the sharp edge, whereas the adjacent black diamonds (shifted along the x axis for clarity) are for the smooth edge.

the second lowest branch, beyond which energies form a continuum. A few points for $N = 36$ deviate slightly from the common trend in the lowest branch, which we believe is due to convergence problems for larger systems.

ii. **Edge Reconstruction**: For $d > d_c$, we observe edge reconstruction due to competing electron-background energy and electron-electron interaction energy.

iii. **Nonlinearity and Edge Rotons**: The lowest branch, though linear at low k, eventually deviates from linearity for all d. We extract in detail the dispersion of the single boson excitation for various d values in Fig. 6, with polynomial fits shown on the plots themselves. We observe that the edge dispersion is nonlinear and the "linearity breakdown" (defined as the point at which the deviation is $\sim$20% from linear) occurs at energies in the range of $0.02 - 0.04(e^2/\epsilon l)$; in experiments, this corresponds to the range 0.2meV to 0.4meV. For $d < d_c \approx 1.5l$, the dispersion also shows a roton structure with the minima around $k_0 = 1.026 l^{-1}$. The roton gap Δ_R is approximately $0.056(e^2/\epsilon l)$ for zero setback distance, but depends on the setback distance and collapses at approximately $d_c = 1.5l$. The analytical fits for the dispersion relations are given in Fig. 5.

The nonlinear dispersion and the existence of the edge roton lie outside the assumptions of the EFTA model. In the next two sections we explore their effect on the edge exponent that is relevant to tunneling into the edge.

V. BOSONIZATION OF FQH EDGE

The bosonic EFTA model is based on the idea that the edge excitations can be mapped into excitations of a bosonic system, given by

$$|\{n_l\}\rangle = \prod_{l=0}^{\infty} \frac{b_l^{n_l}}{\sqrt{n_l!}}|0\rangle , \qquad (13)$$

where n_l is the number of bosons in the orbital with angular momentum l. For a given state $\{n_l\}$, the total angular momentum and total energy are given by

$$\Delta M = \sum_l l\, n_l,$$
$$E_{\{n_l\}} = \sum_l n_l \epsilon_l. \qquad (14)$$

Furthermore, the electron field operator at filling factor $\nu = 1/m$ is given by [2]

$$\hat{\psi}^\dagger(\theta) \propto e^{-i\sqrt{m}\hat{\phi}(x)} = \sqrt{\eta}\, e^{-i\sqrt{m}\hat{\phi}_+(\theta)} e^{-i\sqrt{m}\hat{\phi}_-(\theta)}, \quad (15)$$

where $\sqrt{\eta}$ is a normalization factor. The fields $\hat{\phi}_+(\theta)$ and $\hat{\phi}_-(\theta)$ can be expanded in terms of bosonic creation and annihilation operators b_l and $b_l^\dagger$ as

$$\hat{\phi}_+(\theta) = -\sum_{l>0}\frac{1}{\sqrt{l}} b_l^\dagger e^{il\theta}$$
$$\hat{\phi}_-(\theta) = -\sum_{l>0}\frac{1}{\sqrt{l}} b_l e^{-il\theta}. \qquad (16)$$

A. Electronic and Bosonic edge spectra

We first ask if the excitation spectrum of the electronic problem conforms to the bosonic prediction, in which all excitations are created from a single branch of bosons. Following Ref. [13], we identify the lowest energy state at each angular momentum ΔM in the electronic spectrum with a single boson excitation at $l = \Delta M$, i.e., $n_l = \delta_{l,\Delta M}$. This gives the energy dispersion ϵ_l of the single boson state as a function of l, where we measure the energy ϵ_l with respect to the energy at $\Delta M = 0$ ($M = M_0$). Using the equations $\sum_l l n_l = \Delta M$ and $E_{\{n_l\}} = \sum_l n_l \epsilon_l$, the energies of all the bosonic states $\{n_l\}$ can be obtained and identified with the energies of the corresponding electronic states. We note that in our truncated basis, the numbers of CF and bosonic states are equal at each ΔM.

In Fig. 7, we compare the bosonic excitation spectrum obtained in this manner with the electronic spectra computed through CFD for the edges for the cases $N = 9, 45$ and $d = 0.0$. The CFD spectra are shown in blue circles and the bosonic spectra are shown in red triangles. In all cases, the spectra obtained from the bosonic picture, with the single boson dispersion as an input, show a close resemblance to the electronic spectra, confirming the bosonic picture as well as the interpretation of the lowest branch as the single boson branch. (The bosonic description becomes less accurate with increasing N or ΔM, but still remains accurate for the low-energy states).

B. Spectral Weights

The relation between the electron and the boson operators given in Wen's ansatz in Eq. (1) leads to a precise prediction for the matrix elements of the electron field operator. We will study, following Palacios and MacDonald [Ref. 9], these matrix elements, called spectral weights, defined by

$$C_{\{n_l\}} = \frac{\langle\{n_l\}|\hat{\psi}^\dagger(\theta)|0\rangle}{\langle 0|\hat{\psi}^\dagger(\theta)|0\rangle}, \qquad (17)$$

where $|\{n_l\}\rangle$ represents the bosonic state with occupation $\{n_l\}$, $|0\rangle$ is the vacuum state with zero bosons, $\hat{\psi}^\dagger(\theta)$ is the electron creation operator at position θ (with one dimension wrapped into a circle), and l denotes the single boson angular momentum.

Using Eqs. (1), (16) and (13), it is straightforward to obtain the EFTA predictions for the spectral weights

$$|C_{\{n_l\}}|^2 = \frac{m^{n_1+n_2+\cdots}}{n_1! n_2! \cdots 1^{n_1} 2^{n_2} \cdots}. \qquad (18)$$

We note that the denominator in Eq. (17) eliminates the unknown normalization constant $\sqrt{\eta}$ in Eq. (15).

To obtain the spectral weights from our electronic spectra, we need to identify a "dictionary" between the bosonic states and the electronic states. It is natural to identify the vacuum state $|0\rangle$ with the ground state of interacting electrons at $\nu = 1/m$, denoted by $|\Psi_0^N\rangle$. The field operator has the standard meaning of

$$\hat{\psi}^\dagger(\theta) = \sum_l \eta_l^*(\theta) a_l^\dagger \equiv \sum_l \psi_l^\dagger(\theta), \qquad (19)$$

where $a_l^\dagger$ and a_l are the creation and annihilation operators for an electron in the angular momentum l state, the wave function for which is given in Eq. (4). The wave function $\Psi_{\{n_l\}}^{N+1}(\{z_i\})$ is the electronic counterpart of the bosonic state $|\{n_l\}\rangle$ obtained through CF diagonalization. Using these definitions we calculate the electronic spectral weights. The details of the mapping and calculational method have been discussed in a previously published work [14].
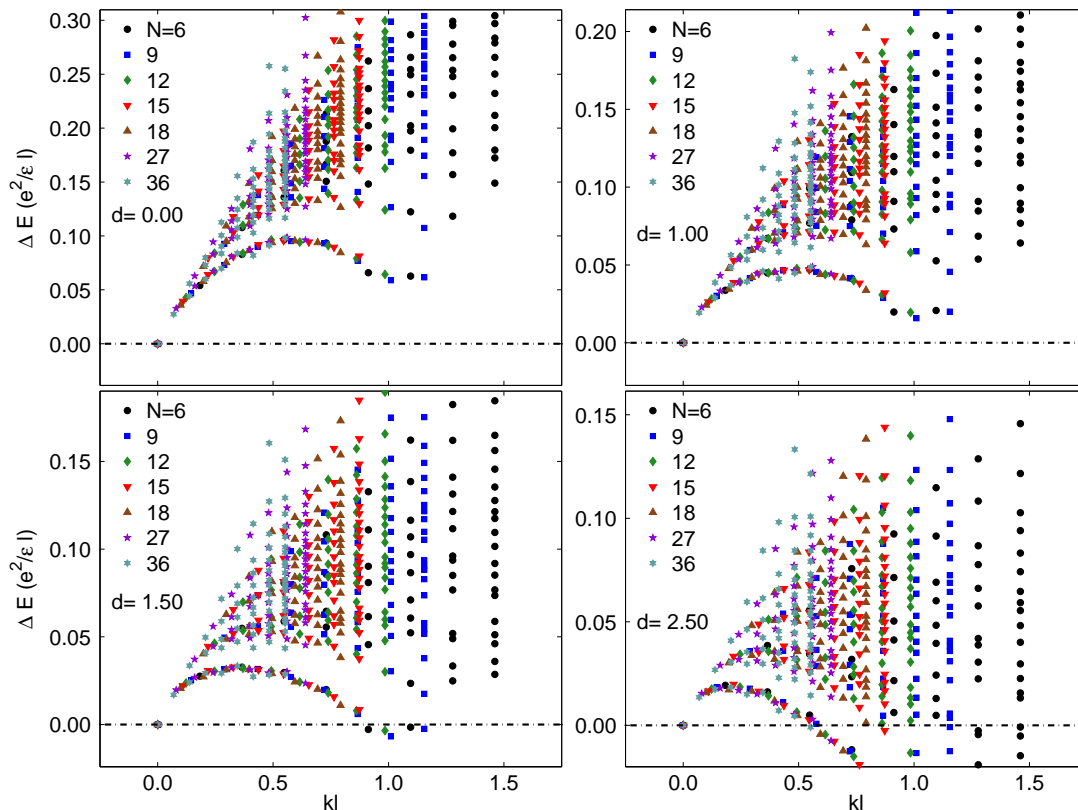
FIG. 5: (Color online) Edge spectra as a function of the physical momentum (see Eq. (12)) for $N = 6 - 36$ particles. The setback distance $d = 0.0 - 2.5l$. Data collapse for the lowest spectral branch can be seen in all the panels. Lower panels with $d \geq 1.5l$ show edge reconstruction.

C. Spectral Weight Sum rules

As seen below, a sum rule for the spectral weights plays an important role. For $\nu = 1/m$, in the bosonic EFTA, the sum of the squared spectral weights (SSW) is given by (see Appendix A for a derivation),

$$
\begin{aligned}
SSW_{\Delta M}^{EFTA} &= \frac{(\Delta M + m - 1)!}{\Delta M!(m-1)!}, \\
\sum_l l n_l &= \Delta M.
\end{aligned} \tag{20}
$$

It is natural to ask whether the above relation holds for the real FQH edge. We test the validity of the sum rules for $\nu = 1/3$ in our model of a FQH edge by computing the spectral weights for system sizes $N = 9 - 27$ and $\Delta M = 1 - 3$. The results for individual spectral weights have been published in a previous work by two of the authors [14]. In Fig. 8, we show the plots of the SSW for Coulomb interactions for different N. The thermodynamic limit for the SSW approaches the expected result according to Eq. (20).

D. A Hybrid Model

To obtain results for the spectral function and the tunneling density of states in the parameter regime of our interest, bigger systems and larger angular momenta are needed. We have found that it is computationally infeasible to calculate the spectra for $N \gtrsim 50$ and $\Delta M \gtrsim 8$, and spectral weights for $N \gtrsim 27$ and $\Delta M \gtrsim 4$. To make further progress we used a hybrid approach. We work with the single boson dispersion obtained by the microscopic theory, but we assume that (i) the full spectrum can be constructed from it by assuming that the bosons are noninteracting, and (ii) the spectral weights of individual states are given by the EFTA model. With these assumptions, our model tests only the effect of nonlinearity of the single boson dispersion. Corrections to the edge exponent arising from coupling to states outside of our restricted basis, as well as those from a redistribution of the spectral weights between states, are outside the scope of our present study.

As an illustration of our hybrid approach, we have plotted in panel (c) of Fig. 9 the spectral weights of various excited states discussed in Sec. V A. The figure illustrates that the spectral weights corresponding to a given number of bosons have roughly the same energy, in agreement
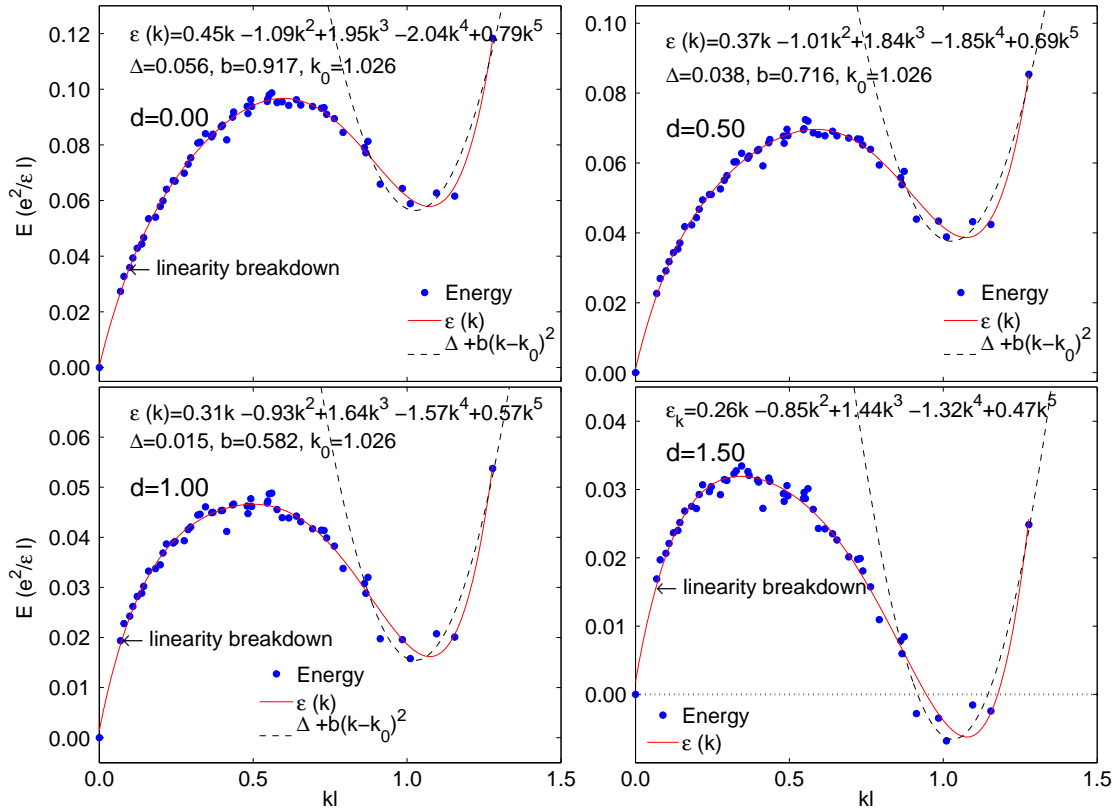
FIG. 6: (Color online) Dispersion $\varepsilon(k)$ of single edge boson for different setback distances in the range $d = 0 - 1.5l$. The solid lines are a fifth order polynomial fit to the lowest branch of the energy spectra in Fig. 5. Arrows indicate the energy beyond which the dispersion becomes nonlinear, as defined in section IV. Dispersion minima for the un-reconstructed edges ($d < 1.5l$) have been fitted with a roton curve $\varepsilon_{roton}(k) = \Delta + b(k - k_0)^2$. Roton gap, momenta and curvature corresponding to the roton minima are also shown. Note that Fig. 5 has d up to $2.5l$, but in this figure we show the plots for the relevant distance range $d = 0 - 1.5l$.
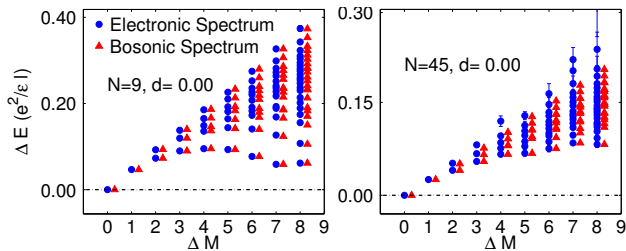

FIG. 7: (Color online) Energy spectrum for the edge excitations of $\nu = 1/3$ (blue dots), obtained by CF diagonalization, for $N = 9, 45$ at $d = 0.0$. Red triangles (shifted along the x axis for clarity) show the bosonic spectra generated from its lowest branch (see section V.A for explanation).

with previous work by Zülicke and MacDonald [15].

VI. SPECTRAL FUNCTION AND TUNNELING DENSITY OF STATES

The positive energy part of the electron spectral function is given by [11,30],

$$A^>(k, E) = \sum_\alpha |\langle \alpha, N+1 | c_k^\dagger | 0, N \rangle|^2 \delta(E - E_\alpha^{N+1} + E_0^N),$$

(21)

where α denotes many-body energy eigenstates, and $k, c_k^\dagger$ denote the momentum (or any other) quantum number and the corresponding electron creation operator respectively. For the FQH edge, if we restrict to the states in the lowest Landau level, $\Psi_{\{n_l\}}^{N+1}(\{z_i\})$ would correspond to $|\alpha, N+1\rangle$. Using the definition of the spectral weight, we can write the spectral function as

$$A^>(k, \epsilon) = \eta \sum_{\{n_l\}} |C_{\{n_l\}}|^2 \delta(\epsilon - E_{\{n_l\}}^{N+1}),$$
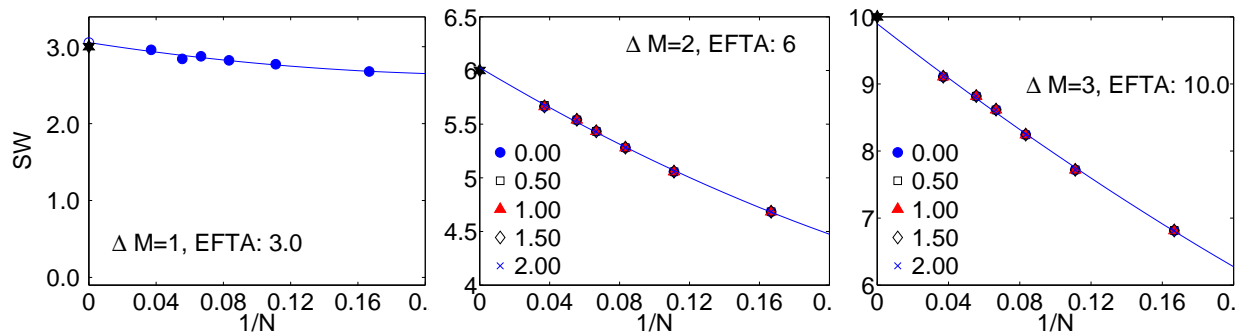
$$\sum_l l n_l = \lambda^{-1} k,$$

(22)

FIG. 8: (Color online) Sum of spectral weights (Eq. (18)) obtained from the electronic spectra (see section V.B for definition) at angular momenta $\Delta M = 1 - 3$ and $d = 0 - 2.0l$. For $\Delta M = 1$, there is only one one state, which is independent of d in our model. For other cases we find that the spectral weight sum is independent of d. Also, the thermodynamic limit is consistent with the sum rule derived from the EFTA (see Eq. (20)).

where $|C_{\{n_l\}}|^2$ is the electronic spectral weight, $E_{\{n_l\}}^{N+1}$ is the energy of the electronic spectra measured from the ground state of $N + 1$ particles, and ϵ is the energy of the edge excitation measured with respect to the chemical potential μ. Here, η is the normalization factor $|\langle 0|\hat{\psi}^\dagger(\theta)|0\rangle|^2$ in Eq. (17). We divide the energy into discrete bins $[\epsilon - \delta/2, \epsilon + \delta/2)$ of width δ and sum over the spectral weights for states with the corresponding energies and momentum k to calculate $A(k, \epsilon)$. As discussed in Sec. V D, we have used the electronic energy dispersion and the bosonic spectral weights to calculate the spectral function.

In Fig. 9, panel (a), we show the energy spectra with spectral weights (colored) for bosonic states. The low-energy states have comparatively smaller weight. The spectral function $A(k, \epsilon)$ (unnormalized and in arbitrary units) for different momenta k are shown in panel (b). In panel (d) we note that the energy corresponding to the maximum of spectral function closely follows the line of maximum energy for a given momenta.

A. Tunneling density of states

When an electron tunnels between two weakly coupled systems (labeled L, R) with a chemical potential difference eV, the tunneling current can be shown to be ([11,30]),

$$I(eV) \sim \sum_{\alpha,\beta} |T_{\alpha,\beta}|^2 \int_0^{eV} dE A_L(\alpha, E) A_R(\beta, eV - E),$$
(23)

where α, β are the quantum numbers of the electron states in the two systems, and $T_{\alpha,\beta}$ is the matrix element connecting the two states. If the energy range of tunneling is small, $T_{\alpha,\beta}$ can be approximated by a constant T independent of the quantum numbers. Further assuming one system (say L) is a metal, whose the density of states is almost constant near the Fermi surface, gives the differential conductance as proportional to the tunneling density of states in the other system (R, labeled as "edge") as

$$\left.\frac{dI}{dV}\right|_{\text{metal}-\text{edge}} \sim D_{\text{edge}}(eV) \equiv \sum_\alpha A(\alpha, E). \qquad (24)$$

For a FQH edge, using Eq. (22), the tunneling density of states (the superscript $N + 1$ is omitted for brevity) is given by,

$$D_{\text{edge}}(\epsilon) \sim \sum_{\{n_l\}} |C_{\{n_l\}}|^2 \delta(\epsilon - E_{\{n_l\}}). \qquad (25)$$

The relation between I and V is given by

$$
\begin{aligned}
I(eV) &\sim \sum_k \int_0^{eV} d\epsilon A^>(k, \epsilon) \\
&\sim \int_0^{eV} d\epsilon \sum_{\{n_l\}} |C_{\{n_l\}}|^2 \delta(\epsilon - E_{\{n_l\}}), \quad (26)
\end{aligned}
$$

which is essentially the sum over all the squared spectral weights of states with excitation energy $\epsilon < eV$ (Ref. [15]).

In Fig. 10, we show the $I - V$ characteristics computed for a system of $N = 75$ particles. Log-log plots in these panels show several plateaus and steps in the low voltage region, which are purely due to the finite size effect of summing over a discrete set of spectral weights (in the low-energy regime we have very few states in spite of the fairly large number of particles considered). We observe, surprisingly in view of the physics described in the introduction, that the exponent α in $I \sim V^\alpha$ remains very close to the ideal EFTA result of 3, within numerical errors. To explore the reasons behind the robustness of the edge exponent to nonlinearities in the dispersion, we have plotted the energy at the maxima of the spectral function $A(k, \epsilon)$ as a function of k in panel (d) of Fig. 9. In the energy region of interest ($\epsilon \leq 0.2$), the peaks roughly follow the ideal EFTA line. The low-energy states near the lower edge of the dispersion have comparatively less spectral weight, and their contribution to the tunneling density of states is negligible.
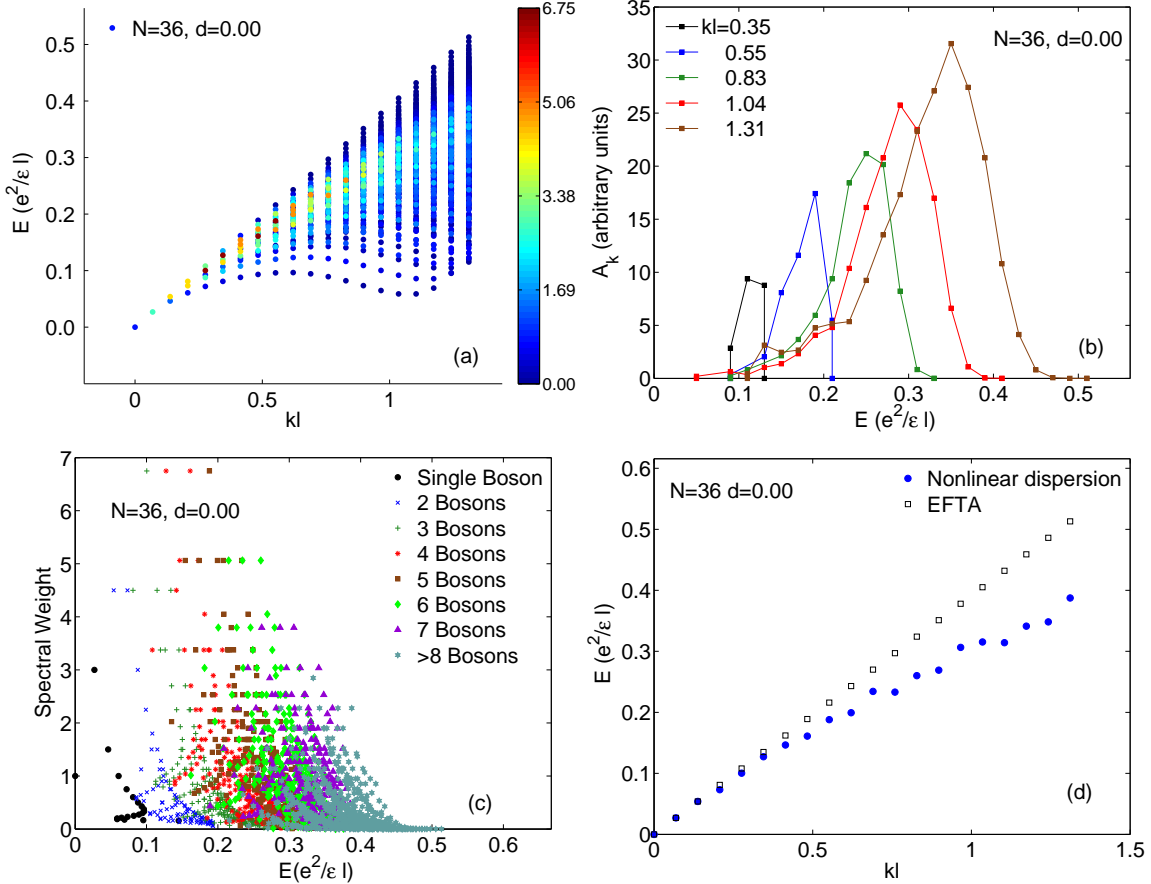
FIG. 9: (Color online) (a) Bosonic spectra generated through electronic dispersion for $N = 36$ particles and $d = 0.0$ using the hybrid approach described in Sec. V.D; the bosonic spectral weights are shown in graduated colors. (b) Spectral function calculated from Eq. (22) for different k using the data in panel (a). (c) Bosonic spectral weights plotted as a function of the energy, grouped by the number of bosons. (d) Energy at the maxima of the spectral function for different k. The black empty squares indicate the situation for a linear dispersion corresponding to EFTA. The system has $N = 36$ particles; the setback distance is $d = 0.0$; and we have restricted to angular momentum up to $\Delta M_{max} = 19$.

B. Irrelevance of edge roton in tunneling

One might ask whether the edge roton produces any signature in a tunneling experiment. In panel (a) of Fig. 10, no significant structure is seen when eV is equal to the roton energy. Panel (b) corresponds to the setback distance where the roton gap just vanishes. Again, there is no prominently visible structure that may be attributed to the roton energy. An increase in the density of states at very low energies, shown in the log-log plots, is associated with the edge roton, but such a signature would be difficult to detect in experiments. We surmise that the spectral weight in the roton mode is too small for it to be observable in tunnel transport.

VII. EFFECTIVE APPROACH FOR RECONSTRUCTED EDGE AND TUNNELING EXPONENT

For systems which undergo edge reconstruction (in our case $d > d_c$), a logical procedure would be to study the excitations around the *new* ground state which now occurs at a finite ΔM. This, however, is not possible in our numerical calculations because of computational limitations. For example, in the 27 or 45 particle system, we cannot go to large enough values of ΔM to identify the minimum energy.

To make further progress, we make the assumption that the edge-reconstructed system can be described by multiple chiral edges (we take three chiral edges below), which interact with one another. For want of a better description, we further assume that each chiral edge can be modeled by the EFTA Lagrangian and ask to what extent this can describe the experiments.

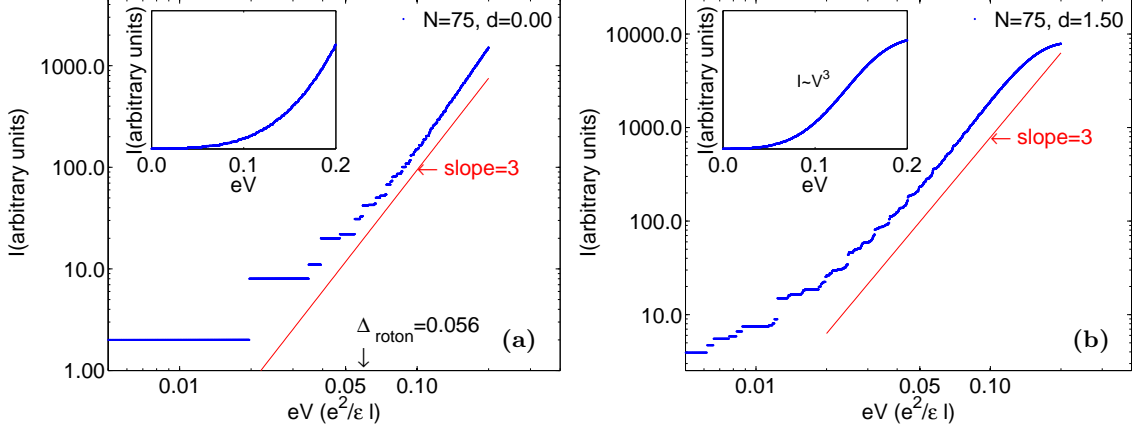We will use the technique of bosonization to study the

FIG. 10: (Color online) (a) The inset shows I as a function of V for tunnel transport between a FQH edge and a Fermi liquid computed from Eq. (26) using the numerical edge dispersion for $N = 75$ particles. The main panel shows the log-log plot of $I - V$ characteristics, to better bring out the power law behavior. The red line marks the curve $I \propto V^3$. The step like deviations at small energies are a finite size artifact (see text for explanation). A logarithmically small deviation can be seen at $eV = \Delta_{\mathrm{roton}}$, the position of which has been marked. (b) Same as in panel (a) but for a setback distance where the roton gap Δ vanishes. The resulting slope is still close to 3 at energies $\epsilon < 0.15$.

effects of density-density interactions between three chiral modes. A model with three modes (two of them moving in one direction and the other mode moving in the opposite direction) is motivated by the analysis in Refs. [31,32]. We denote the modes as 1, 2 and 3, of which 1 and 3 move to the right (from $x = -\infty$ to ∞) and 2 moves to the left (from $x = \infty$ to $-\infty$). We take the bosonic Lagrangian density for the system to be of the EFTA form (we use a slightly different normalization for the bosonic field in this section than in Sec. V),

$$\mathcal{L} = -\frac{1}{4\pi} \int_{-\infty}^{\infty} dx [\sum_{p=1}^{3} \epsilon_p \partial_t \phi_p \partial_x \phi_p + \sum_{p,q=1}^{3} \partial_x \phi_p K_{pq} \partial_x \phi_q],$$
(27)

where $\epsilon_p = 1$ and -1 for the right and left moving fields respectively, and K_{pq} is a real symmetric matrix whose off-diagonal entries give the strengths of the interactions between pairs of modes; we have assumed these interactions to be short-ranged for simplicity. We have absorbed the velocities v_p of the modes in the diagonal parameters K_{pp}. For repulsive density-density interactions, the diagonal elements K_{pp} as well as K_{13} are positive, while K_{12} and K_{23} are negative; this is because the densities of fields 1 and 3 are given by $(1/2\pi)\partial_x \phi_1$ and $(1/2\pi)\partial_x \phi_3$, while the density of field 2 is $-(1/2\pi)\partial_x \phi_2$. Note that the filling factors ν_p ($p = 1, 2, 3$) have not been introduced in the Lagrangian density in Eq. (27). They will appear later when we consider the electron creation operator on edge p, namely, $\psi_p \sim e^{i\phi_p/\sqrt{\nu_p}}$.

To quantize the above theory, we impose the equal-time commutation relations $[\phi_p(x), \rho_q(y)] = -i\delta_{pq}\delta(x - y)$. These are satisfied if the fields have the decomposi-

tion at time $t = 0$,

$$\phi_p(x) = \int_0^{\infty} \frac{dk}{k} [b_{pk} e^{i\epsilon_p kx} + b_{pk}^{\dagger} e^{-i\epsilon_p kx}],$$
(28)

where $[b_{pk}, b_{qk'}^{\dagger}] = \delta_{pq} \, k \, \delta(k - k')$.

In the absence of off-diagonal interactions (i.e., $K_{pq} = 0$ if $p \neq q$), the velocities of the three modes are given by K_{11}, $-K_{22}$ and K_{33}; the first and third are positive, while the second one is negative. When the off-diagonal interactions are present, the Lagrangian density in Eq. (27) can be diagonalized either by a Bogoliubov transformation [33] or, equivalently, by solving the equations of motion. In the latter method, we assume that the fields take the form $\phi_p = X_{p\alpha} e^{ik(x - \tilde{v}_\alpha t)}$, where the index α ($= 1, 2, 3$) labels the three different solutions, and $\tilde{v}_\alpha$ denote the corresponding velocities. The equations of motion then show that the eigenvectors $X_{p\alpha}$ (which are real) and the velocities $\tilde{v}_\alpha$ are solutions of the equations

$$\sum_{q=1}^{3} \epsilon_p K_{pq} X_{q\alpha} = \tilde{v}_\alpha X_{p\alpha}.$$
(29)

We again assume that the new velocities $\tilde{v}_\alpha$ are positive for $\alpha = 1, 3$ and negative for $\alpha = 2$, and we define $\epsilon_\alpha = 1$ for $p = 1, 3$ and -1 for $\alpha = 2$. The eigenvectors $X_{p\alpha}$ can be normalized so that

$$\sum_{p=1}^{3} \epsilon_p \epsilon_\alpha X_{p\alpha} X_{p\beta} = \delta_{\alpha\beta},$$

$$\sum_{\alpha=1}^{3} \epsilon_p \epsilon_\alpha X_{p\alpha} X_{q\alpha} = \delta_{pq}.$$
(30)

If b_{pk} and $\tilde{b}_{\alpha k}$ denote the original and new (Bogoliubov transformed) bosonic annihilation operators, we find that these are related as

$$\tilde{b}_{\alpha k} = \sum_{p=1}^{3} X_{p\alpha} [\frac{1}{2}(1 + \epsilon_p \epsilon_\alpha) b_{pk} - \frac{1}{2}(1 - \epsilon_p \epsilon_\alpha) b_{pk}^\dagger],$$

$$b_{pk} = \sum_{\alpha=1}^{3} X_{p\alpha} [\frac{1}{2}(1 + \epsilon_p \epsilon_\alpha) \tilde{b}_{\alpha k} + \frac{1}{2}(1 - \epsilon_p \epsilon_\alpha) \tilde{b}_{\alpha k}^\dagger].$$

(31)

Using Eq. (30), we can verify that $[b_{pk}, b_{qk'}] = 0$ and $[b_{pk}, b_{qk'}^\dagger] = \delta_{pq} \, k \, \delta(k - k')$ imply that $[\tilde{b}_{\alpha k}, \tilde{b}_{\beta k'}] = 0$ and $[\tilde{b}_{\alpha k}, \tilde{b}_{\beta k'}^\dagger] = \delta_{\alpha\beta} \, k \, \delta(k - k')$, as desired.

Let us now consider the electron creation operator on one of the three edges, say, $\psi_1 \sim e^{i\phi_1/\sqrt{\nu_1}}$, where we have assumed that edge 1 is associated with the filling factor ν_1. In the absence of the off-diagonal interactions, ψ_1 has the scaling dimension $1/(2\nu_1)$. In the presence of interactions, we find from Eq. (31) that the scaling dimension of ψ_1 is given by

$$d_1 = \frac{(X_{11})^2 + (X_{12})^2 + (X_{13})^2}{2\nu_1}.$$

(32)

Since the second equation in Eq. (30) with $p = q = 1$ implies that $(X_{11})^2 - (X_{12})^2 + (X_{13})^2 = 1$, the expression in Eq. (32) is larger than $1/(2\nu_1)$ if $X_{12} \neq 0$, i.e., if there is a non-zero interaction K_{12} between modes 1 and 2. We thus see that interactions between two counter-propagating modes lead to an increase in the scaling dimension of the electron operator; hence the exponent for the two-point correlation function for electrons becomes larger than $1/\nu_1$. In particular, if an edge corresponds to a filling factor of $1/3$ or less, the electron correlation exponent on that edge will be larger than 3. Thus a model with multiple chiral modes in which counter-propagating edges interact with each other has difficulty in explaining the results of tunneling experiments [4–7] which measure an exponent of about 2.7.

Wan *et al* [13] and Joglekar *et al* [34] also studied the reconstruction of FQH edges at $\nu = 1/3$ and showed that the presence of counter-propagating edges leads to a non-universal exponent. Yang [31] introduced an action which has cubic and quartic terms in bosonic fields and showed that this leads to an exponent slightly larger than 3. In contrast, we have considered a standard action which is quadratic in bosonic fields and have shown that interactions between counter-propagating modes necessarily leads to an exponent larger than 3.

VIII. DISCUSSION AND CONCLUSIONS

We have investigated the influence of nonlinear dispersion on the physics of the FQH edge at $\nu = 1/3$. Our approach involves microscopic calculations of the edge dispersion and the associated bosonic spectra, and the use of spectral weights from the bosonic theory.

The conclusions of our work are as follows.

i. The edge dispersion is linear for energies below $0.02 - 0.04 e^2/\epsilon l$ (0.2meV to 0.4meV) depending on the electron-background separation. For $d < d_c = 1.5l$, an edge magnetoroton is observed. The maximum roton gap is $\Delta \approx 0.056(e^2/\epsilon l)$ for zero setback distance.

ii. Edge reconstruction occurs beyond a critical electron-background separation $d_c \approx 1.5l$ for smooth edges of a $\nu = 1/3$ system, in agreement with the previous literature [13].

iii. A bosonic description of the edge excitation spectrum is satisfactory. It requires the dispersion of the single boson excitation as an input.

iv. The spectral weights of the electronic dispersion, though individually different from that of predictions of the bosonic theory, obey the same sum rules for a given angular momentum (provided Λ level mixing is neglected).

v. The tunneling exponent is surprisingly insensitive to the nonlinearity in the edge boson dispersion. The peaks of the spectral function for different momenta roughly follow the linearity of the ideal EFTA. The low-energy states have a small spectral weights and contribute negligibly to the tunneling.

vi. The roton has no significant contribution to the spectral function and hence to the tunneling density of states. Only a logarithmically weak signature of the roton may be observed in tunneling experiments.

vii. It is well known that the model assuming a single chiral mode is not adequate for understanding the results of experiments on systems which undergo edge reconstruction. An effective theory description with three chiral edges at $\nu = 1/3$ produces an exponent that is larger than 3, contrary to the experimental finding of a smaller-than-3 exponent.

IX. ACKNOWLEDGMENTS

X.   APPENDIX

A.   Sum rules

The derivation of the sum rules in Eq. (20) for squared spectral weights at a given angular momenta $\sum_{\{n_l\}} ln_l = M$ is given below. Consider the multinomial expansion (Ref. [18] p. 823)

$$\left(\sum_{k=1}^{\infty} \frac{x_k t^k}{k}\right)^m = m! \sum_{n=m}^{\infty} \sum_{\{a_j\}} \frac{t^n}{n!} \frac{n! \prod_i x_i^{a_i}}{\prod_j (a_j! j^{a_j})},$$
$$\sum_j j a_j = n, \tag{33}$$

With the following transformations

$$\begin{aligned} m &\rightarrow b \quad \text{number of bosons,} \\ x_k &\rightarrow m \quad \text{inverse filling factor,} \\ a_j &\rightarrow n_j \quad \text{bosons occupation,} \\ n &\rightarrow M \quad \text{angular momentum,} \end{aligned}$$

we obtain

$$\left(\sum_{k=1}^{\infty} \frac{m t^k}{k}\right)^b = b! \sum_{M=b}^{\infty} \sum_{\{n_j\}} \frac{t^M}{M!} \frac{M! \prod_i m^{n_i}}{\prod_j (n_j! j^{n_j})},$$
$$\sum_j j n_j = M. \tag{34}$$

Hence we get

$$\sum_{b=0}^{\infty} \left(\frac{1}{b!} \sum_{k=1}^{\infty} \frac{m t^k}{k}\right)^b = \sum_{b=0}^{\infty} \sum_{M=b}^{\infty} \sum_{\{n_j\}} t^M \prod_j \frac{m^{n_i}}{n_j! j^{n_j}} \tag{35}$$

We simplify this by noting the relation

$$\exp\left(m \sum_{k=1}^{\infty} \frac{t^k}{k}\right) = e^{-m \ln(1-t)} = \frac{1}{(1-t)^m}. \tag{36}$$

The sum of the squared spectral weights [9] is the coefficient of t^M

$$\sum_{\{n_l\}} |C_{\{n_l\}}^{(m)}|^2 = \frac{(M+m-1)!}{M!(m-1)!}, \quad \sum_l ln_l = M. \tag{37}$$

B.   Green's function

The ideal EFTA assumes a linear dispersion $\epsilon(k) = v_F k$, and the sum rule in Eq. (37). The Green's function

for the 1D chiral edge is

$$\begin{aligned} G(x,t) &= \langle 0|T(\Psi(x,t)\Psi^\dagger(0,0))|0\rangle \\ &= \langle 0|e^{-iHt} e^{ik0} \Psi(0,0) e^{-ikx} e^{iHt} \Psi^\dagger(0,0)|0\rangle, \ t > 0. \end{aligned} \tag{38}$$

We map the edge to a disk by setting $x = R\theta$ with radius $R = 1$ and insert a complete set of states within the subspace of single boson modes:

$$\sum_M \sum_{\{n_l\}} |M, \{n_l\}\rangle\langle M, \{n_l\}| = I_s; \quad M = \sum_l ln_l. \tag{39}$$

We make the following substitutions

$$\begin{aligned} k &= \lambda M; \quad \lambda = M/\sqrt{6(N-1)} \\ \epsilon_{\{n_l\}} &= \sum_l \epsilon_l n_l = \lambda v_F \sum_l ln_l = \lambda v_F M, \end{aligned} \tag{40}$$

and proceed to calculate the Green's function:

$$\begin{aligned} G(x,t) &= \sum_M \sum_{\{n_l\}} e^{-ikx} \langle 0|\Psi(0,0) e^{iHt}|M, \{n_l\}\rangle \\ &\qquad \times \langle M, \{n_l\}|\Psi^\dagger(0,0)|0\rangle \\ &= \sum_M \sum_{\{n_l\}} e^{-i\lambda M(x-v_F t)} |\langle M, \{n_l\}|\Psi^\dagger(0,0)|0\rangle|^2 \\ &= \sum_M e^{-i\lambda M(x-v_F t)} \sum_{\{n_l\}} |\langle M, \{n_l\}|\Psi^\dagger(0,0)|0\rangle|^2 \\ &= \sum_M e^{-i\lambda M(x-v_F t)} \binom{M+m-1}{m-1} \\ &\sim \frac{1}{(x-v_F t)^m}. \end{aligned} \tag{41}$$

This shows how the power law follows from a combination of the linear dispersion and the sum rule. For a general dispersion ω_k, we evaluate the commutators of the bosonic fields to find the Green's function for the edge:

$$G(x,t) = \frac{2\pi}{L} e^{m \sum_k \frac{1}{k} e^{-i(kx-\omega_k t)} e^{-ak}}. \tag{42}$$

[1] D. C. Tsui, H. L. Stormer, and A. C. Gossard, Phys. Rev. Lett. **48**, 1559 (1982).

[2] X. G. Wen, Int. J. Mod. Phys. B **6**, 1711 (1993).

[3] X. G. Wen, Phys. Rev. Lett. **64**, 2206 (1990).

[4] A. M. Chang, L. N. Pfeiffer, and K. W. West, Phys. Rev. Lett. **77**, 2538 (1996).

[5] M. Grayson, D. C. Tsui, L. N. Pfeiffer, K. W. West, and A. M. Chang, Phys. Rev. Lett. **80**, 1062 (1998).

[6] A. M. Chang, M. K. Wu, C. C. Chi, L. N. Pfeiffer, and K. W. West, Phys. Rev. Lett. **86**, 143 (2001).

[7] A. M. Chang, Rev. Mod. Phys. **75**, 1449 (2003); M. Grayson, Solid State Commun. **140**, 66 (2006).

[8] S. S. Mandal and J. K. Jain, Solid State Communication **118**, 503 (2001); Phys. Rev. Lett. **89**, 096801 (2002).

[9] J. J. Palacios and A. H. MacDonald, Phys. Rev. Lett. **76**, 118 (1996).

[10] F. D. M Haldane, Phys. Rev. Lett. **51**, 605 (1983).

[11] J. K. Jain, *Composite Fermions* (Cambridge University Press, Cambridge, 2007).

[12] R.B. Laughlin, Phys. Rev. Lett.,**50**, 1395 (1983).

[13] X. Wan, E. H. Rezayi, and K. Yang, Phys. Rev. B **68**, 125307 (2003); X. Wan, K. Yang, and E. H. Rezayi, Phys. Rev. Lett. **88**, 056802 (2002).

[14] S. Jolad and J. K. Jain, Phys. Rev. Lett **102**, 116801 (2009).

[15] U. Zülicke and A. H. MacDonald, Phys. Rev. B **54**, R8349 (1996).

[16] A. Imambekov and L. I. Glazman, Science **323**, 228 (2009).

[17] A. Imambekov and L. I. Glazman, Phys. Rev. Lett. **102**, 126405 (2009).

[18] M. Abramowitz and I. A. Stegun, *Handbook of Mathematical Functions* (Dover, New York, 1972).

[19] M. Grayson, M. Huber, M. Rother, W. Biberacher, W. Wegscheider, M. Bichler, and G. Abstreiter, Physica E **25**, 212 (2004).

[20] O. Ciftja and C. Wexler, Phys. Rev. B **67**, 075304 (2003).

[21] E. V. Tsiper, J. Math. Phys. **43**, 1664 (2002).

[22] J. K. Jain, Phys. Rev. Lett. **63**, 199 (1989).

[23] G. S. Jeon, C.-C. Chang, and J. K. Jain, Eur. Phys. J. B **55**, 271 (2007).

[24] J. K. Jain and R. K. Kamilla, Int. J. Mod. Phys. B **11**, 2621 (1997).

[25] G. Dev and J. K. Jain, Phys. Rev. B **45**, 1223 (1992).

[26] J. K. Jain and T. Kawamura, Europhys. Lett. **29**, 321 (1995).

[27] N. Metropolis, A. W. Rosenbluth, M. N. Rosenbluth, A. M. Teller, and E. Teller, J. Chem. Phys. **21**, 1087 (1953).

[28] W. K. Hastings, Biometrika **57**, 1317 (1970)

[29] S. Chib and E. Greenberg, American Statistician **49**, 327 (1995).

[30] For reviews, see: G. D. Mahan, *Many Particle Physics*, third edition (Plenum, New York, 2000); G. F. Giuliani and G. Vignale, *Quantum Theory of Electron Liquid* (Cambridge University Press,Cambridge, 2005).

[31] K. Yang, Phys. Rev. Lett **91**, 036802 (2003).

[32] D. Orgad and O. Agam, Phys. Rev. Lett **100**, 156802 (2008).

[33] C. Tsallis, J. Math. Phys. **19**, 277 (1978).

[34] Y. N. Joglekar, H. K. Nguyen, and G. Murthy, Phys. Rev. B **68**, 035332 (2003).